IEEE Access
Multidisciplinary ⋮ Rapid Review ⋮ Open Access Journal

Received September 26, 2020, accepted October 15, 2020, date of publication October 20, 2020, date of current version November 2, 2020.

Digital Object Identifier 10.1109/ACCESS.2020.3032620

A Methodology to Determine the Effect of a Novel Modulation in the Reliability of an Automotive DC-Link Capacitor

DAVID CABEZUELO ROMERO[1], IÑIGO KORTABARRIA[1], JON ANDREU[1], FERNANDO RODRÍGUEZ[2], ADRIÁN ARCAS[2], AND NICOLA DELMONTE[3], (Senior Member, IEEE)

[1]Department of Electronic Technology, University of the Basque Country (UPV/EHU), 48013 Bilbao, Spain
[2]Aluminium and Film Capacitors Business Group, TDK Electronics Components S. A. U., 29590 Malaga, Spain
[3]Dipartimento di Ingegneria e Architettura, University of Parma (UNIPR), 43124 Parma, Italy

Corresponding author: David Cabezuelo Romero (david.cabezuelo@ehu.eus)

This work was supported in part by the Government of the Basque Country through the Fund for Research Groups of the Basque University System IT978-16 and by the Government of the Basque Country through the Research Program ELKARTEK as the Project ENSOL2 under Grant KK-2020/00077, and in part by the collaboration of TDK.

ABSTRACT Switched Reluctance Machines (SRM) are considered promising rare-earth free candidates for the next generation electrified vehicles. One of the main drawback of this technology is the need of a large DC-link capacitor to balance the energy transferred back and forth between the DC source and the SRM. There are interesting novel modulations to reduce the current of the DC bus, focused on the capacitor size and cost reduction but leaving aside the thermal analysis and lifetime improvements. Carrying out the required dynamic multi-physics simulations for that purpose becomes highly time consuming and complex, especially when standardized or real driving conditions are needed to be taken into account. This article proposes a simulation methodology, simple to implement and with a relatively low computational cost, to estimate the lifetime of an automotive DC-link capacitor, with the current load it delivers as the starting point. The presented methodology has also been used to validate a novel SRM modulation technique and to compare it, in terms of reliability, with the conventional torque sharing function.

INDEX TERMS Switched reluctance motors, capacitor current reduction, electrothermal analysis, reliability, capacitor lifetime.

I. INTRODUCTION

The Electric Vehicle (EV) and the Hybrid Electric Vehicle (HEV) are attracting close attention of consumers, policy-makers and the automotive sector in response to the growing concern and societal awareness over the global warming of our planet and the need to protect the environment.

The electric machine of an EV is one of its most relevant components. Permanent Magnet Synchronous Machines (PMSMs) have been traditionally considered as appropriate candidates for EVs and, specially, for HEVs applications, due to a number of features such as high power density, high efficiency and reliability [1]–[3]. However, these technologies require high density magnetic materials to produce the rotor flux [4], usually sintered neodymium-iron-boron (NdFeB) alloys, and other rare-earth materials, such as dysprosium (Dy), leading to high price risk of depletion and resource monopoly issues [5], [6]. All this makes it necessary to address rare-earth free alternatives.

Among the existing rare-earth free electric machine technologies, the Switched Reluctance Machines (SRMs) are considered promising candidates for the next generation electrified vehicles [7]–[9], due to their flexibility of control, high efficiency, simple structure, low cost and robustness to run under failure conditions [10]–[12].

Nonetheless, some factors are still conditioning a more widespread adoption of SRM-based traction systems [14], such as the complex control due to its no-lineal features and the pulsed nature of its excitation current (derived in torque ripple, vibrations and noise), affecting negatively in the performance of the electric machine. Above all these, the large amount of magnetic energy stored in the windings

The associate editor coordinating the review of this manuscript and approving it for publication was Yunfeng Wen.

This work is licensed under a Creative Commons Attribution 4.0 License. For more information, see https://creativecommons.org/licenses/by/4.0/

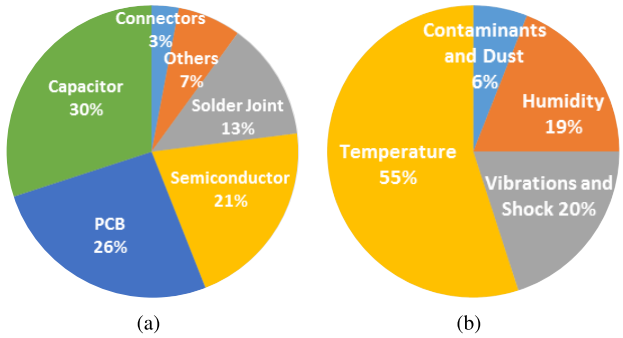

FIGURE 1. Distributions of (a) faults in power converter (b) stress sources [13].

(which is transferred back and forth between the DC source and the SRM through the power converter, causing considerable current peaks [15]) is an important pitfall to overcome. This fact calls for larger DC-link capacitors, increasing the costs and volume of the system and, consequently, negatively affecting the power density. As shown in Fig. 1, DC-link capacitors are one of the main reasons why power converters fail (30 %), being the high temperature the main stress source (50 %) [13]. In consequence, the correct dimensioning of the capacitors is one of the main key issues to designing power converters.

In this context, the automotive industry and political and social agents are forcing the current technology of electric drives to its limits. Within this respect, the technological targets proposed by Horizon 2020, the United States Council for Automotive Research (USCAR), the U.S. Department of Energy (DoE) and the United Nations Economic and Social Commission for Asia (UN ESCAP) regarding the power electronics are stringent. Specifically, the DoE goals for 2020 propose the development of power converter technologies with power density of more than 13.4 kW/l, efficiencies greater than 97 % and a significant cost reduction up to 3.3 $/kW [16].

Indeed, nowadays most SRM-related research focuses on new converter topologies or control improvements. One key method to improve the DC-link performance is to employ a more complex converter topology [17]–[19]. However, these topologies require more devices, reduce the fault tolerance and increase the total volume. A way to reduce the DC-link current with no changes in either the converter or the machine is by means of the control, e.g. just as is done in [20], [21] or [22]. Nonetheless, these proposals use FEM non-linear magnetic models (not considering the degradation or construction errors) or/and need a large computational capability.

Likewise, [23] proposes a method to take advantage of a phenomenon which favors the magnetic energy exchange between phases, and [24] applies the method to develop a technique which aims to maintain a constant average DC-link current over a switching cycle. An enhanced modulation scheme has been published in [14], named Synchronized Switching Modulation (SSM), which takes advantage of the phenomenon synchronizing the phases during the overlap which favors the magnetic energy exchange between phases, thus decreasing the DC bus – SRM energy transfer.

The approach of [14] has two main benefits. On the one hand, the current peaks that DC-link capacitors must sink/source are significantly mitigated, which makes it possible to use lower capacitance, i.e. smaller capacitors, thus increasing power density and reducing costs. On the other, Joule-effect conduction losses drop, which relaxes cooling requirements and improves overall system efficiency. This novel modulation algorithm yields an average reduction of the current of 16 %, allows a capacitance reduction of 20.8 % and improves the overall efficiency of the system up to 6 %. Furthermore, the SSM scheme lets to easily apply it to any kind of current control and is independent of the structural design.

Nevertheless, there is still another aspect not taken into account in [14]. This current reduction, provided by the use of the SSM, decreases the thermal stress and affects directly to the life-cycle of the capacitor. As mentioned (see Fig. 1), the lifetime of a capacitor is very important and necessary to be considered in the design of the complete system, and thermal stress caused by current is a critical stressor to capacitor wear out [25].

Within this context, it is fundamental to define a methodology to predict the lifetime of a capacitor from the current load profile it delivers. A way to quantify the reliability is through the mean time to failure ratio [26]–[28]. Although it is based on the part count method, it can also use information of the application environment. However, it does not consider the real thermal stress.

In the literature, different studies to evaluate the life-cycle can be found on how the DC-link is affected by the temperature and other stresses [29], [30]. Reference [31], e.g., proposes a method to determine reliability issues in automotive power modules combining real-time simulations with electrothermal characterization. Even so, the capacitance and the life-cycle are not taken into account in the analysis, moreover, dynamic multi-physics simulations are highly time consuming and applying them into standardized driving conditions is very complex.

Reference [32] validates a lifetime model for different capacitor technologies (widely used by industry), which uses the two main stressors to capacitor wear out: the hot-spot temperature and the operational voltage. This model is applied within an interesting damage model for a statistical lifetime prediction in an adjustable speed drive [25], a wind power converter [33] and a metro traction drive system [34]. However, these analyze the electrical and thermal behaviour of the capacitor at various static loading conditions, but not at a dynamic real operation cycle. In addition, they need data obtained from repeatedly lifetime testing (of several hundred or thousands of hours, until the failure of the device) with different loading conditions. In consequence, it is a difficult and a too long method to be used in other applications. All

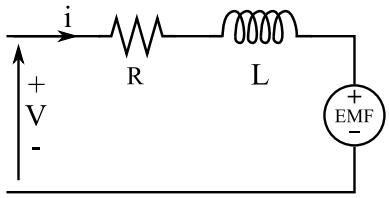

FIGURE 2. Phase equivalent circuit of an SRM.

these methodologies fail in some respect; consequently, they must be combined with other strategies.

Taking the above into account, this article presents two contributions. First, a methodology to estimate the lifetime of a capacitor-pack set into a power converter, starting from the current load that a DC-link delivers into a dynamic load condition. This methodology simplifies the electrothermal simulations taking advantage from the large thermal-inertia that capacitors have, making it simple to implement and with a relatively low computational cost. In addition, the scheme allows to easily apply the methodology to analyze any control which affects the DC-link current. Secondly, the enhanced methodology is employed at the same time to complete the SSM analysis from [14] in a lifetime point of view. The methodology has been developed together with TDK, who has also collaborated in this work providing the automotive DC-link model and its electrothermal simulations.

This article is organized as follows: Section II analyzes the particularities of an SRM, both mathematical modelling and relevant control aspects. Section III exposes the novel SSM scheme in detail, as well as the used validation platform to simulate it. Sections V studies the most suitable capacitor technology for EV application together with the electrothermal and lifetime models used. Then, Section IV presents the standardized driving cycle and the vehicle model used for the simulations. Sections VI-VII describe the proposed methodology and the results obtained of applying it on the SSM, respectively. Finally, Section VIII draws the main conclusions of the work.

II. SRM

A. MATHEMATICAL MODEL

Fig. 2 shows the per-phase equivalent circuit of an SRM, where phase mutual inductances have been neglected for simplicity [35].

From Ohm's and Faraday's laws

$$V = R\,i + \frac{d\psi\,(\theta, i)}{dt}, \tag{1}$$

where R and i are the phase resistance and phase current, and ψ, the magnetic flux, equals

$$\psi = L\,(\theta, i)\;i, \tag{2}$$

which emphasizes that L, the phase self-inductance, depends on both i and θ, the angular position of the rotor. Now, putting together (1)-(2) yields

$$V = R\,i + L\,(\theta, i)\,\frac{di}{dt} + \underbrace{\frac{dL\,(\theta, i)}{d\theta}\omega i}_{\text{EMF}}, \tag{3}$$

where ω is the angular velocity of the rotor.

Finally, from coenergy considerations, the instantaneous per-phase electromagnetic torque can be expressed as

$$T_{em} = \frac{\partial}{\partial\theta}\int \psi\,di = \int \frac{\partial L}{\partial\theta} i\,di = \frac{1}{2} i^2 \frac{dL\,(\theta, i)}{d\theta}. \tag{4}$$

B. CONTROL PARTICULARITIES

Although there are many topologies which meet the requirements of SRM driving, such as phase independence and de/magnetization promptness, the asymmetric H-bridge converter exhibits, above all others, a good controllability over most of the speed range and a high fault tolerance [15], [36], [37]. Fig. 3-① shows a simplified view of the chosen SRM drive, including the power converter stage and the electric machine.

Some control particularities affect to the SRM drive. The most outstanding is that its phases are independent of each other and they must be able to deliver the full rated power to the load individually. Thus, the huge amounts of energy stored in the windings, which are transferred back and forth between the DC bus and the SRM, cause significant current peaks.

A popular way to suppress this fluctuation is to apply a relatively large DC-link capacitor [15], larger than would otherwise be required, in order to act as a buffer that balances the difference of the instantaneous power. However, this solution increases the volume and cost of the converters. Yet the DC bus is, by itself, rather a bulky part, and a major source of faults in modern power converters [13], as well as one of the elements with shortest service of life [2]. Moreover, having to have exceedingly large capacitors makes thing ever worse.

III. SSM – SYNCHRONIZED SWITCHING MODULATION

The enhanced modulation scheme presented in [14], named SSM, takes advantage of a phenomenon which favors the magnetic energy exchange between phases synchronizing them during the overlap, thus decreasing the DC bus – SRM energy transfer. This novel modulation is built 'on top of' a Torque Sharing Function (TSF), and both are implemented into an Indirect Torque Control (ITC).

A. TSF-BASED ITC

The ITC stands out because of its ease of implementation and good cost-to-effectiveness ratio [36], [38], that is why it was chosen as a base to both SSM and TSF modulations. In addition, the following cubic TSF patterns were chosen as a complement because of real-time computation efficiency and

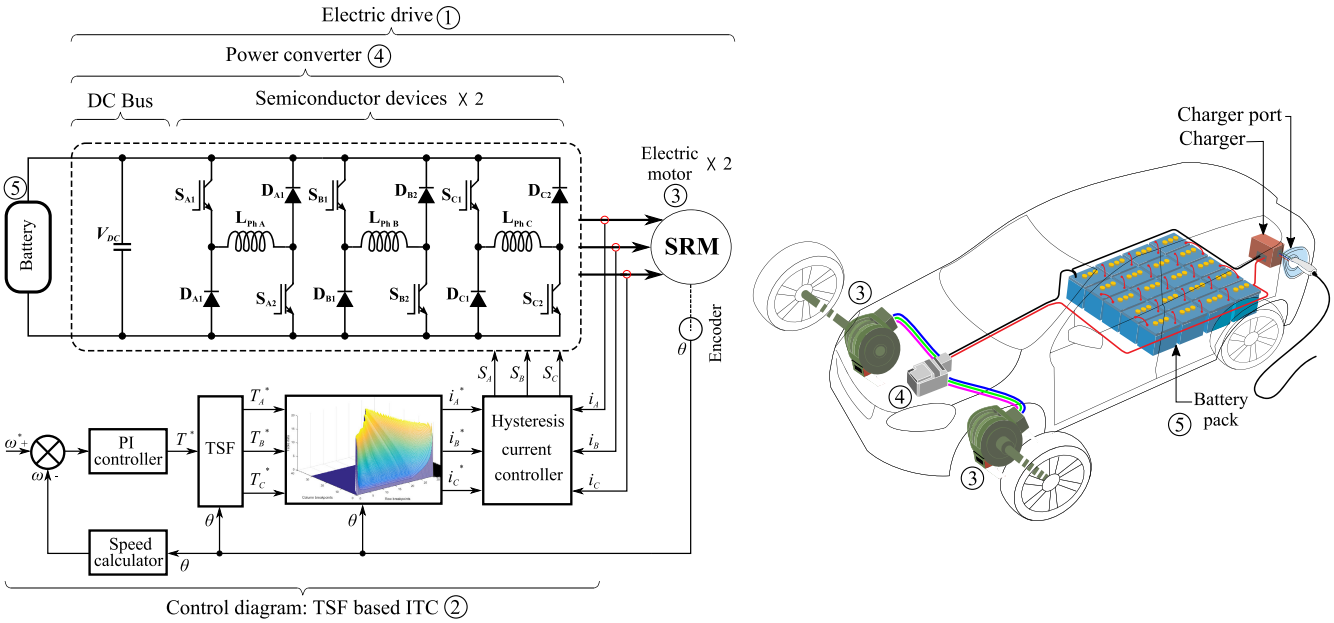

FIGURE 3. Overview of the used automotive electric drive system with its main components.

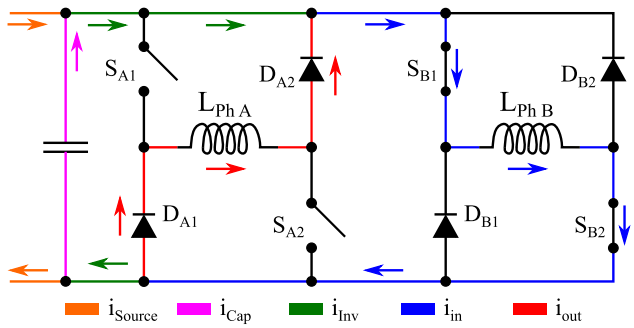

FIGURE 4. Current diagram in a synchronized switching.

low copper loss ratio [14]

$$f_{in}(x) = \begin{cases} 0 & 0 \leqslant \theta < \theta_{on} \\ 3x^2 - 2x^3 & \theta_{on} \leqslant \theta < \theta_{off} \\ 1 & \theta_{off} \leqslant \theta < \theta_T/2 \end{cases} \tag{5}$$

$$f_{out}(x) = \begin{cases} 0 & 0 \leqslant \theta < \theta_{on} \\ 1 - 3x^2 + 2x^3 & \theta_{on} \leqslant \theta < \theta_{off} \\ 1 & \theta_{off} \leqslant \theta < \theta_T/2, \end{cases} \tag{6}$$

where $f_{in}(\cdot)$ and $f_{out}(\cdot)$ stand for the incoming and outgoing patterns respectively, with

$$x \triangleq \frac{\theta - \theta_{on}}{\theta_{ov}}, \quad \theta_{ov} \triangleq \text{overlap angle.}$$

B. SSM DEVELOPMENT

All commutation logic are mutually independent, each follows its own reference and they switch depending on the hysteresis window applied. In spite of that, sometimes commutations do coincide in time (see Fig. 4), and the capacitance current i_{Cap} that the DC bus must sink/source, equals

$$i_{Cap} = i_{Inv} - i_{Source} = i_{in} - i_{out} - i_{Source}, \tag{7}$$

where i_{Inv} is the current provided by the inverter to the phases, i_{Source} the current supplied by the energy source, and i_{in} and i_{out} are the phase magnetizing and demagnetizing currents, respectively.

In order to harness this phenomenon, the SSM forces the synchronization of phase commutation. Hence, one phase must obey the other, i.e. act on a master-slave scheme. Fig. 5 shows the flowchart explaining the SSM logic in detail, only the phase designated as master, i_{out}, is controlled to which the slave phase, i_{in}, is synchronized.

Into the flowchart, i^*_{in} and i^*_{out} are the phase magnetizing and demagnetizing reference currents, respectively, *Hyst* is the hysteresis window considered and m is a parameter introduced at the beginning as a tool to let the hysteresis know about the previous state of the master phase in each iteration — freewheeling or demagnetization.

This scheme allows to easily apply the SSM to any kind of current control. And this approach has two benefits: greatly reduce the capacitance requirements of the DC bus (lower system cost and higher power density and reliability), and improve overall system efficiency (lower cooling requirements). However, the objective of this work is to analyze the effect of the i_{Cap} reduction on the lifetime of the DC-link capacitor. For this purpose, it is essential to define the capacitor's technology.

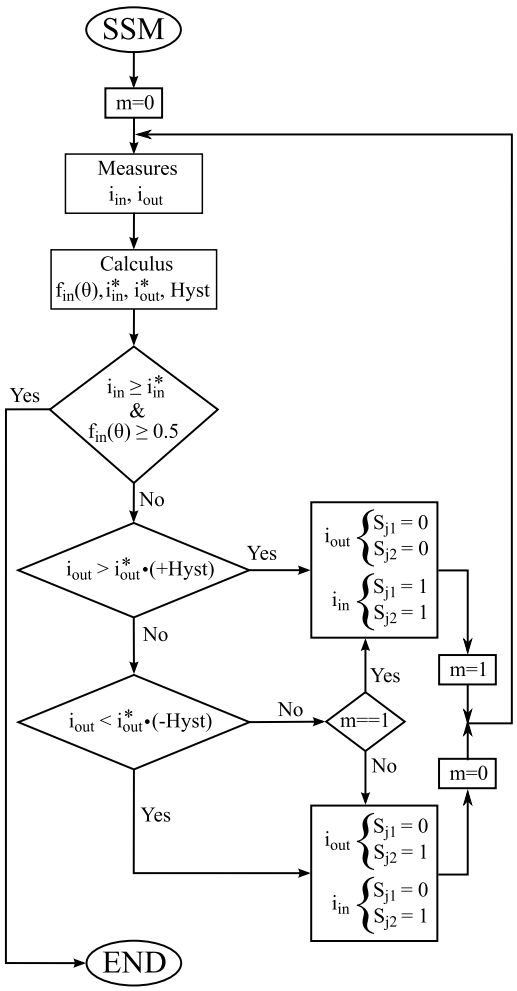

FIGURE 5. SSM flowchart [14].

C. VALIDATION PLATFORM

Fig. 3 displays a general overview of the automotive electric drive system employed to validate by simulation the thermal consequences of the SSM in the lifetime of the DC-link. Fig. 3-② shows the control diagram of the ITC based TSF in which the SSM has been implemented.

The SSM is particularly suitable for a in-wheel SRM without gearbox, where speed is especially low [14]. Therefore, the powertrain is divided into two identical in-wheel SRMs, directly connected to each wheel (see Fig. 3-③ and Table 1) and controlled by the same converter (see Fig. 3-④). Each electric machine phase has its own asymmetric H-bridge; however, they all share the same capacitor.

IV. NEDC AND VEHICLE MODEL

In the last decades, some standardized driving cycles have been proposed to evaluate EVs ensuring realistic results under real operation conditions [39]. Even if the use of the Worldwide Harmonized Light-Duty Vehicles Test Procedure (WLTP) is spreading [31], it is the New European Driving Cycle (NEDC) which is still most widespread, mainly because it is more easy to apply [4]. Therefore, the NEDC was chosen to carry out the simulations. The total duration of the NEDC profile is 1220 s and it is divided into 5 parts (see Fig. 6(a)): 4 repeated ECE-15 Urban Driving Cycles (UDC) and 1 Extra-Urban Driving Cycle (EUDC).

The same backward looking vehicle simulation model as in [4] is used in this work to estimate the required electromagnetic torque. Fig. 7 presents the diagram of this simplified vehicle model, which is divided into two main tasks: the NEDC model generates the vehicle speed profile while the simplified vehicle model uses this reference to obtain the required torque and speed in the wheel. Each electric machine will apply the final transmission torque in order to fulfil the NEDC driving cycle.

TABLE 1. Most significant parameters of the SRM machine.

Parameter	Symbol	Value	Units
Outer diameter	D_o	269	mm
Axial length	l_{en}	155	mm
Peak power	P_P	70	kW
Nominal torque	T_N	400	Nm
Nominal speed	ω_N	1200	rpm
DC side voltage	V_{DC}	400	V
Maximum efficiency	η_{max}	95.2	%
No of stator poles	p_{st}	18	-
No of rotor poles	p_{rt}	12	-
No of phases	ph	3	-

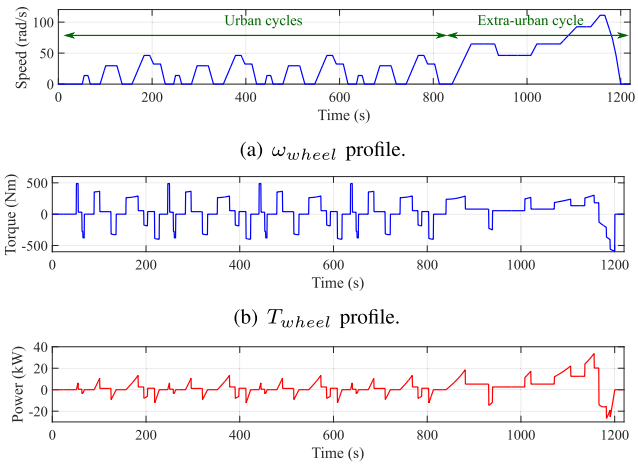

(a) ω_{wheel} profile.

(b) T_{wheel} profile.

(c) Power profile.

FIGURE 6. NEDC profiles for one wheel obtained from the vehicle model.

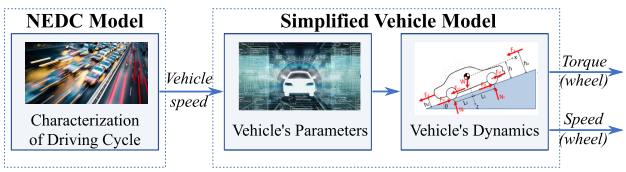

FIGURE 7. Vehicle model for NEDC torque driving cycle profile generation.

TABLE 2. Vehicle parameters used for SRM torque estimation according to the NEDC.

Parameter	Symbol	Value	Units
Vehicle total mass	M_{car}	2800	kg
Rotating mass	M_{rot}	5	%
Vehicle cross section	A_f	3.41	m^2
Wheel radius	r_{wheel}	0.3	m
Gravity acceleration	a_g	9.81	m/s^2
Rolling friction coefficient	μ	0.007	-
Air density	ρ	1.225	kg/m^3
Drag coefficient	C_d	1	-

The required wheels speed and axle torque are given as

$$\omega_{wheel} = \frac{s_{dc}}{r_{wheel}}, \tag{8}$$

$$T_{axle} = r_{wheel}(F_{Roll} + F_{Aero} + F_{Inertia}), \tag{9}$$

where, r_{wheel} is the wheel radius; s_{dc} is the lineal speed of the NEDC driving cycle; and, F_{Roll}, F_{Aero}, and $F_{Inertia}$ are the rolling resistance, aerodynamic resistance, and inertia forces, respectively. These last three can be defined as [4]

$$F_{Roll} = \mu a_g M_{car}, \tag{10}$$

$$F_{Aero} = \frac{\rho s_{dc}^2 C_d A_f}{2}, \tag{11}$$

$$F_{Inertia} = [M_{car}(1 + M_{rot})]\, a_{car}, \tag{12}$$

where M_{car} is the total vehicle mass; a_g is the gravity acceleration; μ is the rolling friction coefficient; ρ is the air density; C_d is the drag coefficient; A_f is the vehicle cross section; M_{rot} is the equivalent mass of the rotating parts of the car (expressed in %); and, a_{car} is the car acceleration defined as ds_{dc}/dt. The grade force was considered in this simplified vehicle model.

Two in-wheel SRMs were used to traction the vehicle, so each wheel must provide only half of the total torque

$$T_{wheel} = \frac{T_{axle}}{2} \tag{13}$$

As the selected in-wheel motor does not need a gearbox, equations (8) and (13) give directly the speed and torque needed in the wheel. This also avoids gearbox and idling losses, making the system more efficient. Regarding the model vehicle parametrization, an electric big van full loaded was defined (Volkswagen e-Crafter), where the most significant parameters are shown in Table 2. The brake blending law in this application is defined as 100 % electric braking. This vehicle model was run offline to obtain the torque and speed curves shown in Fig. 6.

V. AUTOMOTIVE CAPACITOR ANALYSIS

A. CAPACITOR TECHNOLOGY FOR EV APPLICATION

Three types of capacitors are generally used in high voltage DC-link applications, which are the Aluminum Electrolytic Capacitor (Al-Cap), Multi-Layer Ceramic Capacitor (MLC-Cap) and the Film Capacitor (F-Cap). The last one is a wide family that offers multiple options, but within this one the most used technology is the Metallized Polypropylene Film Capacitor (MPPF-Cap) [32].

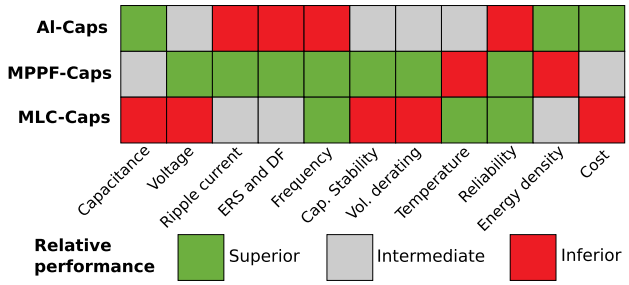

FIGURE 8. Performance comparison of the main types of capacitors for DC-link applications [32].

TABLE 3. i_{Cap} and C_{min} estimations for a complete NEDC cycle.

	i_{Cap} (A_{RMS})	C_{min} (μF)
TSF	10.65	529
SSM	9.27	401

MPPF-Caps have a superior performance Fig. 8 shows a performance qualitative comparison, exhibiting the specific advantages and shortcomings of each technology. MPPF-Caps have a superior performance, they provide a well-balanced performance for high voltage applications (above 500 V) in terms of cost, ESR, capacitance, current ripple and reliability [32]. The cost of MPPF-Caps is about 1/3 of Al-Caps [2]. All this and the possibility to achieve higher power density DC-link designs in high ripple current applications, make the MPPF-Cap technology the preferred to automotive application [2].

B. ELECTION OF THE CAPACITOR

Once the most suitable technology has been chosen, it remains to define the capacitor used to evaluate the two modulations tested. By means of a preliminary simulation in Matlab of the vehicle's speed and torque profiles (see Fig. 6(c)) in a complete NEDC cycle, the i_{Cap} profiles for both modulations have been obtained (see Table 3).

This drop in i_{Cap} makes it possible to also reduce the required capacitance value. However, the selected capacitor should satisfy the needs of the most adverse modulation for a better comparison. The theoretical minimum capacitance value can be quantified by [17]:

$$C_{min} = \frac{L_a i_{Cap}^2}{0.1 V_{DC}^2}, \tag{14}$$

where L_a is the inductance with alienated poles, and V_{DC} is the rated DC bus voltage. The application of the TSF-based ITC resulted in $C_{min} = 529$ μF, whereas the SSM-enhanced ITC yielded $C_{min} = 401$ μF, i.e. a reduction of 24.2 %.

For the capacitor-selecting task, TDK has collaborate providing information of a MPPF-Cap solution specially fitted

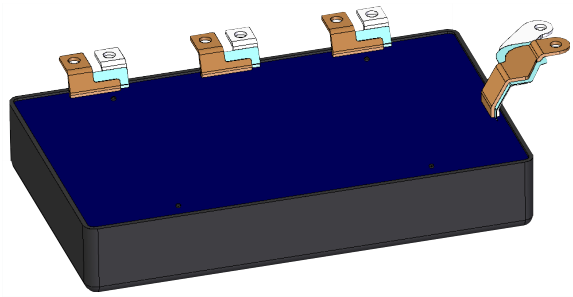

FIGURE 9. 3D outline of TDK's automotive MPPF-Cap.

to the vehicle's power specification. It is a complete DC-link solution as it is made by a capacitor + busbar and connections with the DC battery part and the three-phase inverter (see Fig. 9). Its main parameters are: 550 μF and 450 V of rated capacitance and voltage, respectively.

C. ELECTROTHERMAL MODEL

For the electrothermal simulations two different simulation software were used, depending on the simulation type:

- For electromagnetic simulations, Flux PEEC 2018.1.3 from Altair were used. This is a software which uses Partial Element Equivalent Circuit (PEEC) as the method of its solver, which is a partial inductance calculation method widely used for modelling in Electromagnetics since 70s.
- Thermal simulations were done with ANSYS Mechanical 2019 R3. This is a worldwide leader software, especially for thermal and mechanical simulations. It is based in the Finite Element Method (FEM), which is a numerical technique used to perform Finite Element Analysis (FEA) or any given physical phenomenon.

To transfer results from one to the other, Microsoft Excel was used.

Fig. 10 shows the workflow for the whole (electromagnetic + thermal) capacitor simulations. Stablishing the Boundary Conditions (BC) is essential, both thermal and electrical:

- Thermal BC (see Fig. 10-①). It is mandatory to define always the ambient temperature T_{amb} [40], which represents the temperature of capacitor's surroundings. To improve the simulation, the temperature of certain part of the capacitor can be also defined (e.g. the terminals, or a face by cooling).
- Electrical BC (see Fig. 10-②). Includes the currents that the capacitor is undergoing in the simulation (i.e. i_{Cap}, i_{Source} and phase currents in RMS values, and the spectrum of the first one).
- Structural design (see Fig. 10-③). The structural design of the capacitor is another initial input; in this case it was modelled by CAD.

Electromagnetic simulation block (see Fig. 10-④) refers to the Flux PEEC solver, in the same way as the thermal simulation block (see Fig. 10-⑤) refers to the ANSYS Mechanical solver. The first one has three main outputs: losses distribution (given in volumetric losses W/m^3 for the conductive parts of the capacitor), current distribution (given in A/m^2) and the electrical model as its equivalent circuit (C, R_p ESR and ESL, see Fig. 10-⑥).

Finally, thermal model (see Fig. 10-⑦) and temperature distribution (see Fig. 10-⑧) are obtained from the thermal results, and it is represented as the thermal resistance

$$R_{th} = \frac{\Delta T}{P_{losses}}, \tag{15}$$

where ΔT is the temperature increase from the T_{amb} to the hot-spot temperature T_{ht}, and P_{losses} is the total amount of losses that the capacitor bears.

D. LIFETIME MODEL

Lifetime models [25], [32]–[34] are important for lifetime estimation, online condition monitoring and benchmark of different capacitor solutions.

The estimation of the lifetime of a F-Cap depends on the rate of self-healing events and the energy of each one as the number of operating hours increases [41]. Each self-healing event is followed by a slight drop in the capacitance due to the loss of internal metal surface. The end-of-life criterion of an F-Cap, defined by the IEC61071 standard, is established at the point where the capacitor has lost 3 % of its initial value of capacitance [42].

For F-Caps, a widely used lifetime model is [25], [32]

$$L = L_0 \left(\frac{V_{op}}{V_0}\right)^{-k_1} 2^{\frac{T_{amb}-T_{hs}}{k_2}}, \tag{16}$$

where L, L_0, V_{op} and V_0 are the lifetime under testing conditions, rated lifetime, operation voltage and rated voltage of the capacitor. For film capacitors, the exponent k_1 is from around 7 to 9.4, which is used by leading capacitor manufacturers, and k_2 is a coefficient around 10 [25].

The accumulated damage D is the lifetime complement on a scale of 0 to 1, i.e. a D of 0 would be equivalent to the rated lifetime and an D of 1 would mean that the device has reached its theoretical useful lifetime. The nonlinear D model of [25] is used to describe the real damage progress

$$D = r^q, \tag{17}$$

where r is the ratio l_i/L_i, being l_i and L_i the instantaneous equivalent operating time and total lifetime under the same loading condition, respectively; and q is a function of lifetime which represents the degradation speed of the capacitor under operating condition.

The mayor manifestation of damage into a capacitor is the increase of ESR over time, mainly by the dielectric degradation, naturally caused or by stress (with T_{hs} and V_{op} as the principal stressors (16)). In consequence, the nonlinear damage curve is represented by the ESR increasing curves in the lifecycle, which are obtained from several lifetime testing (until device failure) with different loading conditions.

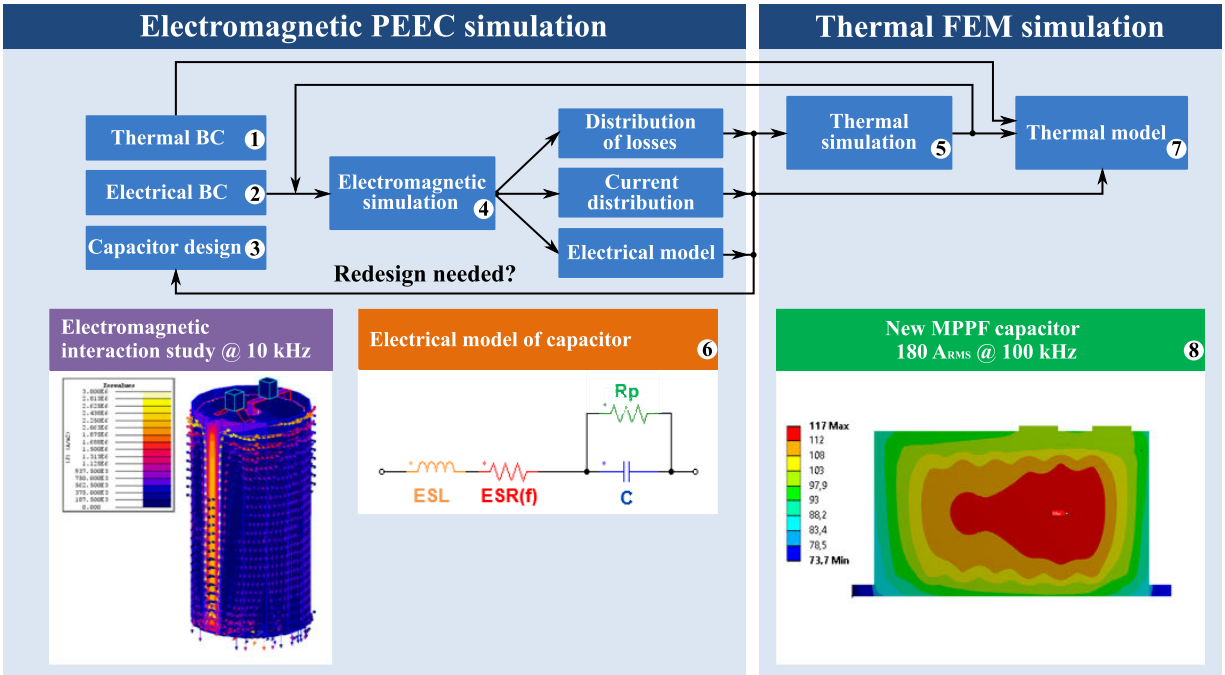

FIGURE 10. Graphical description of the multiphysics simulation workflow.

Because these data are a valuable industrial know-how, manufacturers do not provide this data. In this situation, the linear model-miner rule can be used for fast evaluation making $q = 1$ in (17).

VI. PROPOSED ENHANCED METHODOLOGY

Fig. 11 shows the general diagram of the proposed reliability analysis methodology. The left hand blocks shows the steps to be carried out by Matlab model simulations, while the right hand represent the steps to be carried out by multi-physics simulations. Besides, there are some data processing steps between both groups of blocks. The proposed methodology is divided in the following 8 steps:

1) First, the real driving conditions must be determined (see Fig. 11-①). To do this, the vehicle model and the standardized driving model have been defined in Section IV.

Carrying out a long dynamic multi-physics simulation would require extremely high computational capacity; therefore, it is not feasible to implement it. Further, capacitors have a large thermal-inertia, this means that in the case of applying an operation point (e.g. the maximum power point) it would take hours to achieve thermal stability and would not represent the real operating condition at all (i.e. the capacitor will not operate in high torque areas for hours). This allows to discretize the driving cycle in different points and consider them as a group of static conditions, making possible to simulate them individually.

2) For all this, the selected standardized driving cycle is divided (see Fig. 11-②). 22 different operation regions are defined based on the speed profile of the NEDC (11 dividing the UDC and another 11 dividing the EUDC, as it can be seen in Fig. 12).
3) Then, each region is represented as an operation point ($P_i, \forall\, i \in [1, 22]$) and their mean torque $T_{wheel_{mean}}$ and mean speed $\omega_{wheel_{mean}}$ are calculated (see Fig. 11-③).
4) All the operation points are simulated, each one with its $T_{wheel_{mean}}$ and $\omega_{wheel_{mean}}$, with both modulation techniques to obtain the corresponding i_{Cap}, i_{Source} and phase currents profiles (see Fig. 11-④).

The electrothermal simulation of all the operational points would still take an unbearable amount of time. Simulating and obtaining the thermal model of the two most exigent operational points (P_{ME1} and P_{ME2} from now on) is enough to extrapolate the result to the rest of the points, thus, next two steps are only applied on these.

5) As has been mentioned in Subsection V-C, the electrothermal model needs the i_{Cap} spectrum, so it must be calculated in an intermediate step (see Fig. 11-⑤).
6) Electrothermal simulations are carried out as explained in Subsection V-C (see Fig. 11-⑥ and Fig. 10).
7) From the results of the two most exigent operational points, the rest are calculated by extrapolation (see Fig. 11-⑦). The effect of the frequency in the thermal losses is not negligible; however, in this case most of the current of each operational point is in the same frequency range. This way, the overheating (represented as ΔT) for the rest of the operational points that have not been simulated can be calculated by thermal extrapolation, as shown below.

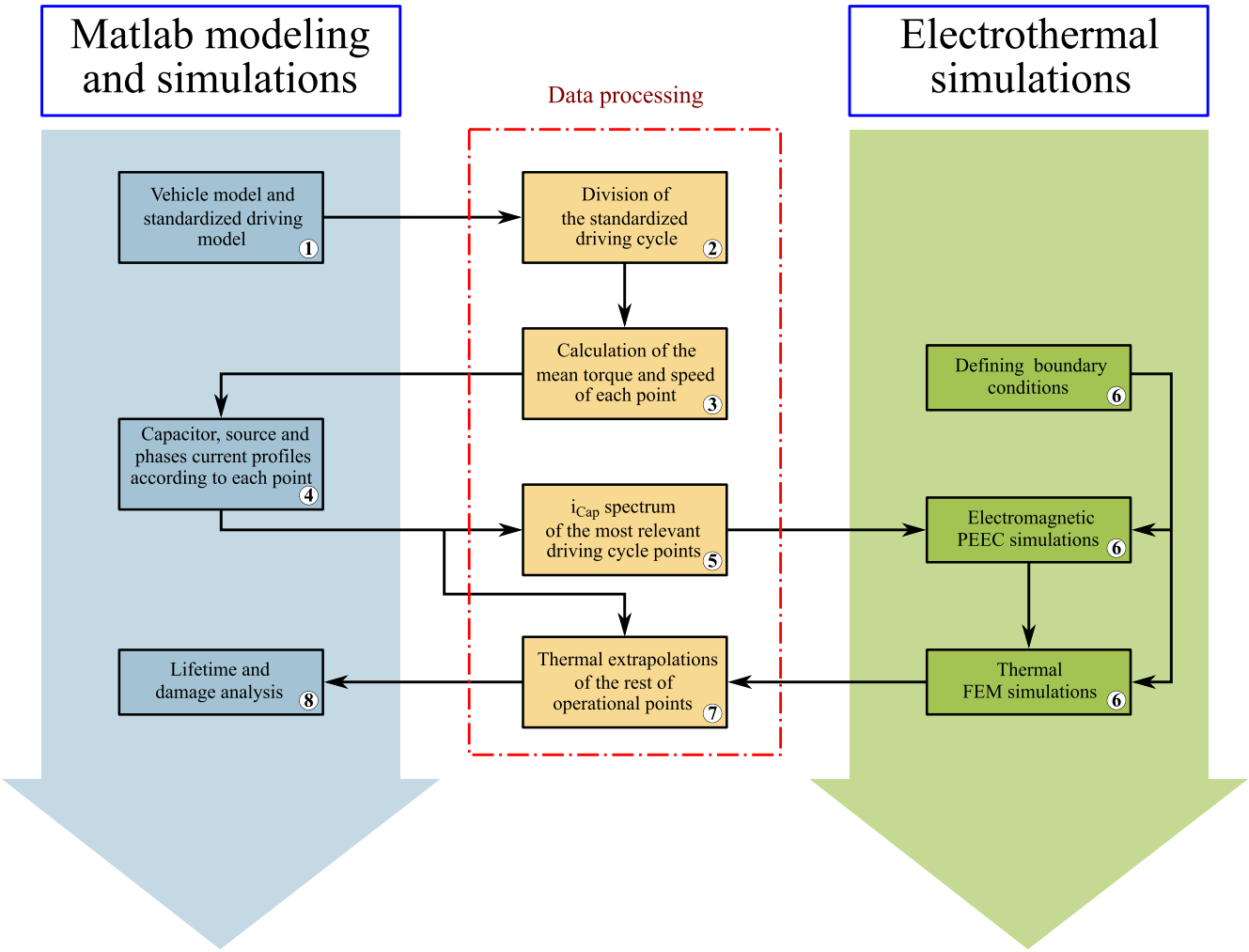

FIGURE 11. General diagram of the proposed methodology to determinate the effect of a modulation in the reliability of a DC-link.

Firstly, the R_{th} for P_{ME1}&P_{ME2} is calculated independently for the TSF and the SSM as seen in (15). Then, for each remaining operational point, their losses are calculated as

$$P_{losses_{Pxx}} = P_{losses_{P_{ME1}}} \left(\frac{i_{Tot_{Pxx}}}{i_{Tot_{P_{ME1}}}} \right)^2, \qquad (18)$$

where $P_{losses_{Pxx}}$ and $i_{Tot_{Pxx}}$ are the losses and the total current in RMS (i.e. the sum of i_{Cap}, i_{Source} and phase currents in RMS values) for each operational point, respectively. At last, having each operational point's losses, ΔT is obtained directly multiplying those losses by the R_{th} of the corresponding modulation.

8) Finally, to determine the lifetime change with each modulation technique, all the operation points are taking into account considering the time period of each one (see Fig. 11-⑧). As well as the periods with the vehicle at standstill.

This scheme allows to easily apply the simulation methodology to any kind of control.

TABLE 4. General data of P20 and P22.

	i_{Cap} (A_{RMS}) TSF	SSM	$\omega_{wheel_{mean}}$ (rad/s)	$T_{wheel_{mean}}$ (Nm)
P20	106.6	88.3	101.4	137,9
P22	107.2	95.5	66.2	-164,1

VII. LIFETIME ANALYSIS OF THE SSM

The enhanced methodology will now be applied to complete the SSM analysis. As was justified in Section VI, in order to further simplify the computational load to an assumable simulation time, from the 22 operation points that have been defined (see Fig. 12), only the two most exigent were simulated electrothermally (P20 and P22). The 20 remaining points were calculated by extrapolation from the result of the two simulated ones.

In Table 4, general results of steps ③ and ④ (see Fig. 11) can be seen for P20 and P22. Fig. 13 shows the discrete

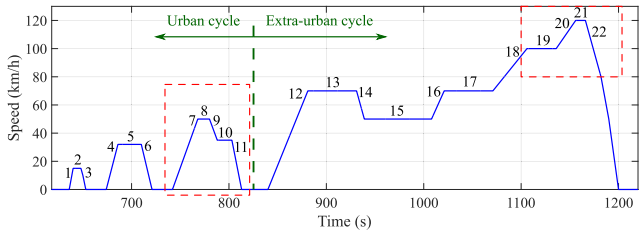

(a) Speed profile.

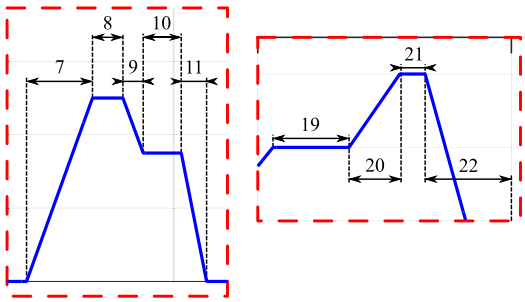

(b) (c)

FIGURE 12. NEDC profile region division, with two zooms a) and b).

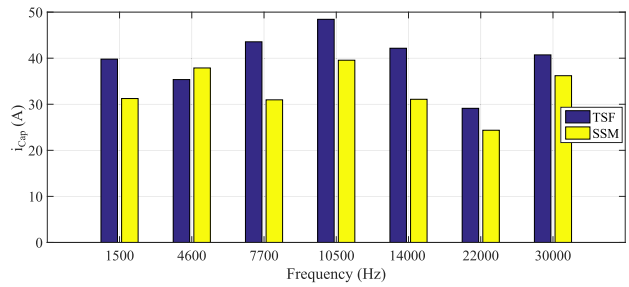

(a) P20 point.

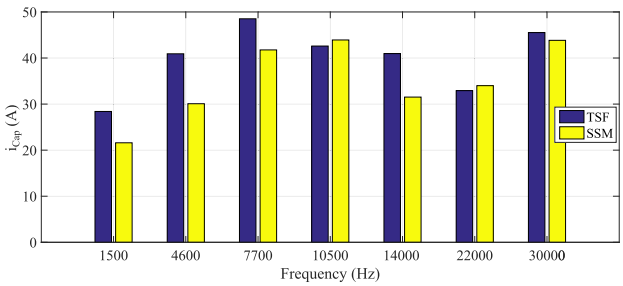

(b) P22 point.

FIGURE 13. i_{Cap} spectrum for both TSF-based and SSM-enhanced ITC.

current spectrum of step ⑤ used in the electrothermal model for these operational points.

A. TEMPERATURE RESULTS AND THERMAL EXTRAPOLATIONS

The electrothermal simulations and extrapolations have been carried out with the collaboration of TDK.

Common automotive capacitor materials have been used for these simulations: metallized polypropylene film for the capacitive elements, copper for the stripes that joint these capacitive elements, polymer case and epoxy resin potting. For the simulation, the following thermal BC have been established (common in automotive application):

- Phase terminals temperature: fixed at 90 °C.
- Convection: a typical natural convention air coefficient of 10 W/(m^{2}K) is assumed, with a T_{amb} of 90 °C.

Obtained thermal maps, provided by ANSYS Mechanical software, have the same scale so comparisons are easier and clearer. The T_{hs} at P22 with the TSF is 105.3 °C (see Fig. 14) and with the SSM is 100.1 °C (see Fig. 15). As it can be seen, internally the DC-link is made by paralleling 5 capacitive elements. In both cases, this T_{hs} corresponds to the first one (from left to right, see Fig. 14(a) and Fig. 15(a)). This is caused by the internal construction and wiring pattern, more current is concentrated in the left side and, in consequence, more thermal losses occur.

Comparing both modulations at the P22 operational point, the capacitor would be overheated around 5.2 °C less with the SSM, achieving a ΔT reduction of a 34 % (see Table 5). While at P20 it would be 4.1 °C less of overheat and a ΔT reduction of a 28.7 %, obtaining a similar thermal map (see Fig. 16 and Fig. 17).

From the results of P20 and P22, the temperatures of the rest of the operational points have been calculated by extrapolation as defined in step ⑦ (see Fig. 11). For that purpose, firstly the R_{th} for P20 and P22 is calculated obtaining a value around 0.77 °C/W and 0.74 °C/W for the TSF and the SSM, respectively. Table 5 summarizes all the results for both TSF and SSM.

TABLE 5. Temperatures for each operational point. In bold the simulated ones.

	TSF		SSM		ΔT reduction
	T_{hs} (ºC)	ΔT (ºC)	T_{hs} (ºC)	ΔT (ºC)	(%)
P01	100.8	10.8	97.6	7.6	-29.4
P02	90.12	0.12	90.07	0.07	-45.6
P03	94.2	4.2	92.9	2.9	-31.9
P04	97.5	7.5	95.1	5.1	-31.0
P05	90.09	0.09	90.05	0.05	-44.3
P06	96.0	6.0	94.0	4.0	-34.4
P07	94.9	4.9	93.1	3.1	-36.2
P08	90.2	0.21	90.1	0.13	-40.9
P09	91.9	1.9	91.1	1.1	-39.3
P10	90.05	0.05	90.03	0.03	-44.5
P11	100.9	10.9	97.1	7.1	-34.7
P12	94.9	4.9	93.1	3.1	-37.9
P13	90.4	0.43	90.3	0.26	-40.4
P14	94.8	4.8	92.8	2.8	-41.0
P15	90.14	0.14	90.08	0.08	-40.7
P16	96.6	6.6	94.0	4.0	-38.4
P17	90.4	0.43	90.3	0.26	-40.8
P18	95.2	5.2	93.2	3.2	-38.8
P19	92.0	2.0	91.1	1.1	-43.3
P20	**104.3**	**14.3**	**100.2**	**10.2**	**-28.7**
P21	95.3	5.3	93.1	3.1	-41.7
P22	**105.3**	**15.3**	**100.1**	**10.1**	**-34.0**

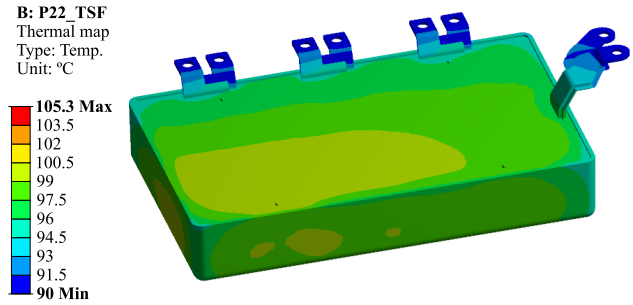

(a) General view.

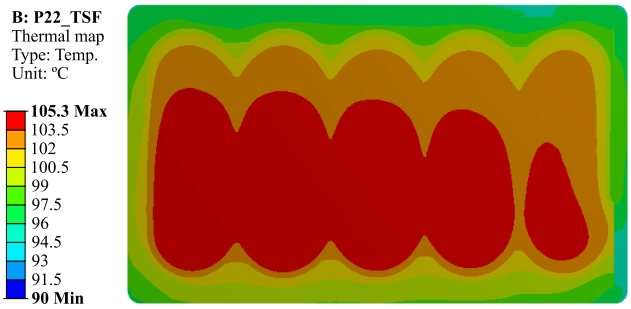

(b) Half-height cross section view.

FIGURE 14. ANSYS thermal simulation of the P22 operational point with TSF-based ITC.

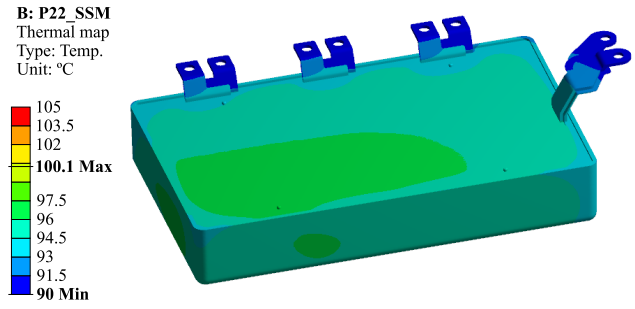

(a) General view.

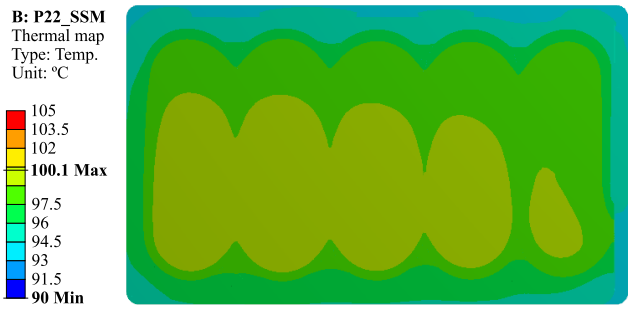

(b) Half-height cross section view.

FIGURE 15. ANSYS thermal simulation of the P22 operational point with SSM-enhanced ITC.

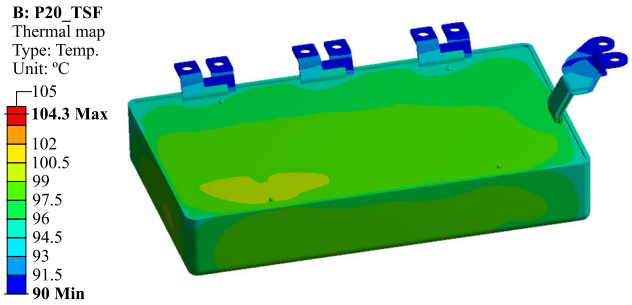

(a) General view.

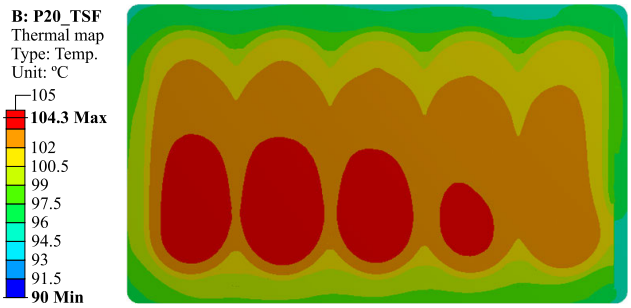

(b) Half-height cross section view.

FIGURE 16. ANSYS thermal simulation of the P20 operational point with TSF-based ITC.

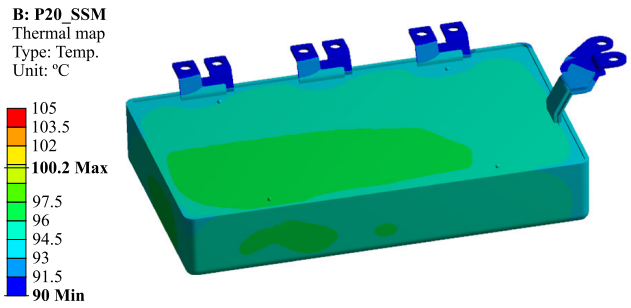

(a) General view.

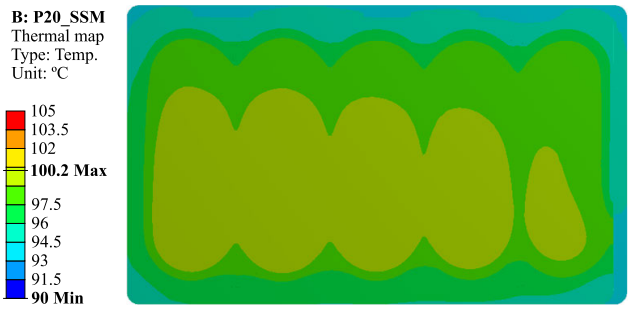

(b) Half-height cross section view.

FIGURE 17. ANSYS thermal simulation of the P20 operational point with a SSM-enhanced ITC.

B. LIFETIME ANALYSIS

Applying the T_{hs} data of Table 5 into the lifetime model (considering $V_{op} = 400$ V constant) to calculate L_i, and using it together with the known l_i of each operation point within the linear damage model, it can be estimated how many NEDC cycles the EV will be able to perform until D reaches a value of 1 (rated lifetime). Doing this, with both TSF-based and SSM-enhanced ITCs, and comparing the results allows to know the real impact of the i_{Cap} reduction.

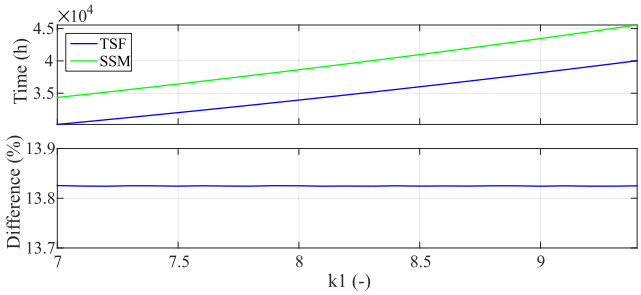

FIGURE 18. Lifetime estimation results for both TSF-based and SSM-enhanced ITC.

For a correct calculation of the lifetime model, k_1 must be defined, but this constant is characteristic for each F-Cap and, in consequence, manufacturers do not provide it either. However, as it will be seen, it is not necessary to define it to make a comparison, since the porcentual difference between both modulations remains constant for any k_i value.

Fig. 18 compares the results obtained. For a $k_1 = 8$ the lifetime estimation with the TSF-based ITC resulted in 33940 h, whereas the SSM-enhanced ITC yielded in 38630 h, i.e. an increase of 13.83 %. Moreover, this increasing is maintained in all the k_1 values.

VIII. CONCLUSION

This article has presented a novel methodology to determine reliability issues in automotive DC-link capacitors. This methodology simplifies the complex and long dynamic multiphysics simulation process to estimate the lifetime of an automotive capacitor taking into account the current load it delivers. The NEDC has been used as the standardized driving cycle, but it could also be implemented with any other driving test procedure.

The methodology can be also used as a basis for a rapid method to select the capacitor based on the lifetime target for a specific application. Capacitors are usually selected by the maximum DC-link voltage ripple, but the lifetime can be also added as a selecting factor. Different capacitors can be analysed comparing their lifetimes under the same load condition. The electrothermal model of the used capacitor is still needed, but not the *ESR* degradation curves, thus simplifying the whole process.

At the same time, an enhanced SRM modulation, called Synchronized Switching Modulation (SSM), has also been validated to test its influence in the hot-spot temperature and the lifetime of the DC-link, compared with the classic torque sharing function. Such comparison have shown that the reduction of i_{Cap} with the SSM was enough to achieve a 13.83 % of lifetime increasing. Besides that, it would also allow a reduction in capacitance by 24.23 %, making possible to choose depending on the objectives.

These results are promising, and make the SSM an interesting modulation technique for SRMs. The SSM is particularly suitable for heavy-duty applications or in-wheel without gearbox, that's why the employed experimental platform is based into a two in-wheel powertrain system. However, the SSM could also be implemented along with other modulation schemes in central motor-equipped EVs, by combining the SSM with other modulation schemes in an adaptive fashion.

ACKNOWLEDGMENT

This work has been carried out inside the UPV/EHU research staff training program (2015).

REFERENCES

[1] T. Jahns, "Getting rare-earth magnets out of EV traction machines: A review of the many approaches being pursued to minimize or eliminate rare-earth magnets from future EV drivetrains," *IEEE Electrific. Mag.*, vol. 5, no. 1, pp. 6–18, Mar. 2017.

[2] I. López, E. Ibarra, A. Matallana, J. Andreu, and I. Kortabarria, "Next generation electric drives for HEV/EV propulsion systems: Technology, trends and challenges," *Renew. Sustain. Energy Rev.*, vol. 114, pp. 1–23, Oct. 2019.

[3] J.-R. Riba, C. López-Torres, L. Romeral, and A. Garcia, "Rare-earth-free propulsion motors for electric vehicles: A technology review," *Renew. Sustain. Energy Rev.*, vol. 57, pp. 367–379, May 2016.

[4] E. Trancho, E. Ibarra, A. Arias, I. Kortabarria, P. Prieto, I. M. de Alegría, J. Andreu, and I. López, "Sensorless control strategy for light-duty EVs and efficiency loss evaluation of high frequency injection under standardized urban driving cycles," *Appl. Energy*, vol. 224, pp. 647–658, Aug. 2018.

[5] N. A. Mancheri, B. Sprecher, G. Bailey, J. Ge, and A. Tukker, "Effect of Chinese policies on rare earth supply chain resilience," *Resour., Conservation Recycling*, vol. 142, pp. 101–112, Mar. 2019.

[6] C. Cox and J. Kynicky, "The rapid evolution of speculative investment in the REE market before, during, and after the rare earth crisis of 2010–2012," *Extractive Ind. Soc.*, vol. 5, no. 1, pp. 8–17, Jan. 2018.

[7] S. Morimoto, S. Ooi, Y. Inoue, and M. Sanada, "Experimental evaluation of a rare-earth-free PMASynRM with ferrite magnets for automotive applications," *IEEE Trans. Ind. Electron.*, vol. 61, no. 10, pp. 5749–5756, Oct. 2014.

[8] E. Oksuztepe, "In-wheel switched reluctance motor design for electric vehicles by using a Pareto-based multiobjective differential evolution algorithm," *IEEE Trans. Veh. Technol.*, vol. 66, no. 6, pp. 4706–4715, Jun. 2017.

[9] J. Zhu, K. W. E. Cheng, X. Xue, and Y. Zou, "Design of a new enhanced torque in-wheel switched reluctance motor with divided teeth for electric vehicles," *IEEE Trans. Magn.*, vol. 53, no. 11, pp. 1–4, Nov. 2017.

[10] A. El-Refaie, T. Raminosoa, P. Reddy, S. Galioto, D. Pan, K. Grace, J. Alexander, and K.-K. Huh, "Comparison of traction motors that reduce or eliminate rare-earth materials," *IET Electr. Syst. Transp.*, vol. 7, no. 3, pp. 207–214, Sep. 2017.

[11] K. V. Singh, H. O. Bansal, and D. Singh, "A comprehensive review on hybrid electric vehicles: Architectures and components," *J. Mod. Transp.*, vol. 27, no. 2, pp. 77–107, Jun. 2019.

[12] I. Boldea, L. N. Tutelea, L. Parsa, and D. Dorrell, "Automotive electric propulsion systems with reduced or no permanent magnets: An overview," *IEEE Trans. Ind. Electron.*, vol. 61, no. 10, pp. 5696–5711, Oct. 2014.

[13] U.-M. Choi, F. Blaabjerg, and K.-B. Lee, "Study and handling methods of power IGBT module failures in power electronic converter systems," *IEEE Trans. Power Electron.*, vol. 30, no. 5, pp. 2517–2533, May 2015.

[14] D. Cabezuelo, I. Kortabarria, J. Andreu, U. Ugalde, B. Blanqué, and P. Andrada, "Synchronized switching modulation to reduce the DC-link current in SRM drives," *IEEE Access*, vol. 8, pp. 57849–57858, Mar. 2020.

[15] S. Li, S. Zhang, T. G. Habetler, and R. G. Harley, "Modeling, design optimization, and applications of switched reluctance Machines—A review," *IEEE Trans. Ind. Appl.*, vol. 55, no. 3, pp. 2660–2681, Jun. 2019.

[16] S. Rogers and S. Boyd, "Overview of the DOE VTO electric drive technologies R&D program," U.S Dept. Energy, Washington, DC, USA, Tech. Rep., Jun. 2016.

[17] W. Cai and F. Yi, "An integrated multiport power converter with small capacitance requirement for switched reluctance motor drive," *IEEE Trans. Power Electron.*, vol. 31, no. 4, pp. 3016–3026, Apr. 2016.

[18] A. Klein-Hessling, B. Burkhart, and R. W. D. Doncker, "Active source current filtering to minimize the DC-link capacitor in switched reluctance drives," *CPSS Trans. Power Electron. Appl.*, vol. 4, no. 1, pp. 62–71, Mar. 2019.

[19] F. Yi and W. Cai, "A Quasi-Z-Source integrated multiport power converter as switched reluctance motor drives for capacitance reduction and Wide-Speed-Range operation," *IEEE Trans. Power Electron.*, vol. 31, no. 11, pp. 7661–7676, Nov. 2016.

[20] T. Kusumi, K. Kobayashi, K. Umetani, and E. Hiraki, "Analytical derivation of phase current waveform eliminating torque ripple and input current ripple of switched reluctance motors under magnetically saturated operation," in *Proc. IEEE Energy Convers. Congr. Expo. (ECCE)*, Sep. 2019, pp. 6540–6547.

[21] F. Yi and W. Cai, "Repetitive control-based current ripple reduction method with a multi-port power converter for SRM drive," in *Proc. IEEE Transp. Electrific. Conf. Expo (ITEC)*, Jun. 2015, pp. 1–6.

[22] H.-N. Huang, K.-W. Hu, and C.-M. Liaw, "Switch-mode rectifier fed switched-reluctance motor drive with dynamic commutation shifting using DC-link current," *IET Electr. Power Appl.*, vol. 11, no. 4, pp. 640–652, Apr. 2017.

[23] C. R. Neuhaus, N. H. Fuengwarodsakul, and R. W. De Doncker, "Control scheme for switched reluctance drives with minimized DC-link capacitance," *IEEE Trans. Power Electron.*, vol. 23, no. 5, pp. 2557–2564, Sep. 2008.

[24] W. Suppharangsan and J. Wang, "Switching technique for minimisation of DC-link capacitance in switched reluctance machine drives," *IET Electr. Syst. Transp.*, vol. 5, no. 4, pp. 185–193, Dec. 2015.

[25] H. Wang, P. Davari, H. Wang, D. Kumar, F. Zare, and F. Blaabjerg, "Lifetime estimation of DC-link capacitors in adjustable speed drives under grid voltage unbalances," *IEEE Trans. Power Electron.*, vol. 34, no. 5, pp. 4064–4078, May 2019.

[26] V. V. S. Pradeep Kumar and B. G. Fernandes, "Switching strategy for improving the lifetime of DC-link capacitor in a fault-tolerant active power decoupling topology," *IET Power Electron.*, vol. 11, no. 1, pp. 52–61, Nov. 2018.

[27] R. Parvari, M. Zarghani, and S. Kaboli, "RCD snubber design based on reliability consideration: A case study for thermal balancing in power electronic converters," *Microelectron. Rel.*, vols. 88–90, pp. 1311–1315, Sep. 2018.

[28] S. Xu, H. Chen, and F. Dong, "Converter-level reliability prediction and analysis in switched reluctance motor drive," *IET Electr. Power Appl.*, vol. 14, no. 3, pp. 500–511, Mar. 2020.

[29] R. Gallay, "Metallized film capacitor lifetime evaluation and failure mode analysis," in *Proc. CAS-CERN Accel. School, Power Converter*, May 2014, pp. 45–56.

[30] A. Gupta, O. P. Yadav, D. DeVoto, and J. Major, "A review of degradation behavior and modeling of capacitors," in *Proc. ASME Int. Tech. Conf. Exhib. Packag. Integr. Electron. Photonic Microsyst.*, Aug. 2018, Art. no. V001T04A004.

[31] A. Matallana, E. Robles, E. Ibarra, J. Andreu, N. Delmonte, and P. Cova, "A methodology to determine reliability issues in automotive SiC power modules combining iD and 3D thermal ssimulation under driving cycle profiles," *Microelectron. Rel.*, vol. 102, pp. 1–9, Nov. 2019.

[32] H. Wang and F. Blaabjerg, "Reliability of capacitors for DC-link applications in power electronic converters—An overview," *IEEE Trans. Ind. Appl.*, vol. 50, no. 5, pp. 3569–3578, Sep. 2014.

[33] D. Zhou, Y. Song, Y. Liu, and F. Blaabjerg, "Mission profile based reliability evaluation of capacitor banks in wind power converters," *IEEE Trans. Power Electron.*, vol. 34, no. 5, pp. 4665–4677, May 2019.

[34] B. Yao, X. Ge, H. Wang, H. Wang, D. Zhou, and B. Gou, "Multitimescale reliability evaluation of DC-link capacitor banks in metro traction drive system," *IEEE Trans. Transport. Electrific.*, vol. 6, no. 1, pp. 213–227, Mar. 2020.

[35] D. S. Mihic, M. V. Terzic, and S. N. Vukosavic, "A new nonlinear analytical model of the SRM with included multiphase coupling," *IEEE Trans. Energy Convers.*, vol. 32, no. 4, pp. 1322–1334, Dec. 2017.

[36] R. Krishnan, *Switched Reluctance Motor Drives: Modeling, Simulation, Analysis, Design, and Applications*. Boca Raton, FL, USA: CRC Press, 2001.

[37] D. Cabezuelo, J. Andreu, I. Kortabarria, E. Ibarra, and I. M. de Alegria, "Power modules for electric vehicles SRM converter," in *Proc. Int. Exhib. Conf. Power Electron., Intell. Motion, Renew. Energy Energy Manage.*, Jun. 2018, pp. 1–7.

[38] K. Chau, *Electric Vehicle Machines and Drives: Design, Analysis and Application*. Hoboken, NJ, USA: Wiley, 2015.

[39] J. Ko, D. Jin, W. Jang, C.-L. Myung, S. Kwon, and S. Park, "Comparative investigation of NO_x emission characteristics from a euro 6-compliant diesel passenger car over the NEDC and WLTC at various ambient temperatures," *Appl. Energy*, vol. 187, pp. 652–662, Feb. 2017.

[40] H. Wang, R. Zhu, H. Wang, M. Liserre, and F. Blaabjerg, "A thermal modeling method considering ambient temperature dynamics," *IEEE Trans. Power Electron.*, vol. 35, no. 1, pp. 6–9, Jun. 2020.

[41] *Application Notes—Power Electronic Capacitors*, EPCOS AG, Munich, Germany, Apr. 2010.

[42] *Film Capacitors—Power Electronic Capacitors, MKP DC Type*, EPCOS AG, Munich, Germany, May 2018.

DAVID CABEZUELO ROMERO received the B.S. degree in mining engineering specialized in energy resources from the University of the Basque Country, Bilbao, Spain, in 2013, and the M.S. degree in energy and power electronics from the University of Mondragon, Mondragon, Spain, in 2015. He is currently pursuing the Ph.D. degree with the Department of Electronic Technology, Applied Electronic Research Team, University of the Basque Country. From 2013 to 2014, he has worked as a Technical Assistant with the University of Mondragon, on energy balancing themes with Li-Ion technology. From 2014 to 2015, he has worked as a Research and Development Technician in Orona, Hernani, Spain, developing a solar-lift solution. His main research interests include electric and hybrid vehicles, variable-speed drives, control strategies, and power converters.

IÑIGO KORTABARRIA received the M.Sc. degree from the University of Mondragon, Mondragon, Spain, in 1999, and the Ph.D. degree from the University of the Basque Country, Bilbao, Spain, in 2013, all in electronics and control engineering. From 1999 to 2004, he was a Research and Development Staff Member in industrial electronics companies. From 2004 to 2014, he was an Assistant Professor in electronic technology with the Department of Electronic Technology, University of the Basque Country. In 2014, he became an Associate Professor. His current research interests include power converters and applications of power electronics.

JON ANDREU received the M.S. degree in electronic and control engineering from the University of Mondragon, Mondragon, Spain, in 1997, and the Ph.D. degree in electronic and control engineering from the University of the Basque Country, Bilbao, Spain, in 2008. He was with the Ideko Research Center, where he was involved in machine tools applications. Since 2002, he has been an Assistant Professor in electronic technology with the Department of Electronic Technology, University of the Basque Country, where he became an Associate Professor in 2011. His current research interests include power converters and applications of power electronics.

FERNANDO RODRÍGUEZ received the M.Sc. degree in electronics from the University of the Basque Country, Spain, in 1999. Since 2001, he has been working with TDK Electronics (formerly EPCOS). He has more than 15 years of experience in capacitor design and development for power electronic applications: HVDC systems, traction, automotive, and renewable energy converters. He is currently in charge of the Applications and Simulation Group, FILM Capacitors. His research interest includes advanced capacitors development for upcoming WBG semiconductor technologies (GaN and SiC mainly).

ADRIÁN ARCAS received the M.Sc. degree in industrial engineering and the master's degree in CAE simulations from the National University of Distance learning (UNED), Spain, in 2013 and 2016, respectively. Since 2017, he has been working with TDK Electronics (formerly EPCOS). He has more than five years of experience in design and development of mechanical systems in aeronautics and industry, and more than two years of experience in simulations of capacitors, specialized in thermal and electromagnetic simulations. He works as a Simulation Engineer with the Research and Development ADG Department, FILM Capacitors.

NICOLA DELMONTE (Senior Member, IEEE) was born in Manfredonia, Italy, in 1967. He received the Laurea degree in electronic engineering and the Ph.D. degree in information technology from the University of Parma, Parma, Italy, in 2002 and 2006, respectively. Since 2002, he has been with the Department of Engineering and Architecture, University of Parma, where he became a Research Fellow in 2005, an Assistant Professor in 2013, and an Associate Professor in 2018. His current research interests include the study of breakdown phenomena and high-field accelerated stress of pHEMTs, the technological processing for RF test structures on thin ceramic films, the electrical and thermal characterization, modeling, reliability evaluation of power devices and hybrid modules, and the design of renewable-energy plants, nanogrids, and smart systems.